SOFT X-RAY MEASUREMENTS IN THE TRIAM-1 TOKAMAK

Satoh, Takemichi
Research Institute for Applied Mechanics, Kyushu University : Graduate Student

Toi, Kazuo
Research Institute for Applied Mechanics, Kyushu University : Associate Professor

Nakamura, Kazuo
Research Institute for Applied Mechanics, Kyushu University : Research Associate

Nakamura, Yukio
Research Institute for Applied Mechanics, Kyushu University : Research Associate

他

https://doi.org/10.5109/6777116

出版情報：Reports of Research Institute for Applied Mechanics. 29 (91), pp.27-48, 1981-07. 九州大学応用力学研究所
バージョン：
権利関係：

Reports of Research Institute for Applied Mechanics
Vol. XXIX, No. 91, 1981

SOFT X-RAY MEASUREMENTS IN THE TRIAM-1 TOKAMAK

By Takemichi SATOH*, Kazuo TOI**, Kazuo NAKAMURA***,
Yukio NAKAMURA***, Naoji HIRAKI***
and Satoshi ITOH****

Soft X-ray pulse height analysis system has been designed and constructed for measurements of electron distribution function and impurity with high spatial resolution (0.5 cm) and temporal resolution (2 msec) in the TRIAM-1 tokamak. The experimental results about electron temperature, enhancement factor, Z_{eff} and runaway electrons are presented and discussed.

Key words: Soft X-ray, TRIAM-1, Pulse height analysis, Impurity, Radial profile, Enhancement factor, Runaway electron

1. Introduction

The radiation loss by bremsstrahlung increases as the plasma temperature and density approach the high temperature and high density of thermo-nuclear fusion plasma. The radiation power P_b lost by bremsstrahlung per unit volume is,

$$P_b \propto Z^2 n^2 T^{1/2}, \tag{1}$$

where Z, n and T are ion charge, density and temperature, respectively. Since P_b increses in proportion to Z^2, the radiation loss due to impurity increases remarkably when it comes into the plasma.

Soft X-ray radiation measurement is one of the methods for radiation loss measurement. The electron temperature can be derived from the energy spectrum of soft X-ray radiation. There are two methods by which we measure the energy spectrum of soft X-ray radiation:

* Graduate Student, Research Institute for Applied Mechanics, Kyushu University. Present address: Hitachi, Ltd.
** Associate Professor, Research Institute for Applied Mechanics, Kyushu University. Present address: Institute of Plasma Physics, Nagoya University.
*** Research Associate, Research Institute for Applied Mechanics, Kyushu University.
**** Professor, Research Institute for Applied Mechanics, Kyushu University.

1) pulse height analysis method,
2) absorber method.

The former method can measure electron energy distribution function with high accuracy. Therefore not only measurement of T_e but also the identification of the impurity species are possible. And the quantity of impurities can be determind by measuring the effective ion charge Z_{eff}.

Pulse Height Analysis system (PHA system) has been constructed for energy spectrum measurement of soft X-ray radiation from the TRIAM-1 tokamak plasma. In this report the design of the PHA system and the results of energy spectrum measurements of soft X-ray radiation are described.

2. Soft X-ray radiation processes and principle of measurement

2.1. Soft X-ray radiation processes

The main radiation processes of soft X-ray from high-temperature plasma are as follows:

a) Bremsstrahlung by collision between electrons and ions,
b) Recombination radiation between electrons and ions,
c) Line radiation from impurity except the working gas,
d) Dielectronic recombination radiation.

The influence of line radiation and dielectronic recombination radiation is removable because of discontinuity in energy spectrum. Therefore we consider bremsstrahlung and recombination radiation in this subsection.

Energy spectra of soft X-ray radiation by bremsstrahlung $(\Delta I/\Delta E)_{ij}^{ff}$ and recombination $(\Delta I/\Delta E)_{ij}^{fb}$ for Maxwellian plasma are as follows[1]:

$$\left(\frac{\Delta I}{\Delta E}\right)_{ij}^{ff} = 3\times10^{-15} n_e n_{ij} (Z_{ij}^{ff})^2 \frac{\overline{g_{ff}}}{\sqrt{T_e}} \exp\left(-\frac{E}{T_e}\right) (\mathrm{cm^{-3}\,sec^{-1}}), \tag{2}$$

$$\left(\frac{\Delta I}{\Delta E}\right)_{ij}^{fb} = 3\times10^{-15} n_e n_{ij} (Z_{ij})^2 \frac{\overline{g_{fb}}}{\sqrt{T_e}} \exp\left(-\frac{E}{T_e}\right) \times \left[\frac{\xi}{n^3}\frac{\chi_{ij}}{T_e}\exp\left(\frac{\chi_{ij}}{T_e}\right) + \sum_{\nu=1}^{\infty}\frac{2\chi_H}{T_e}\frac{(Z_{ij})^2}{(n+\nu)^3}\exp\left\{\frac{(Z_{ij})^2}{(n+\nu)^2}\frac{\chi_H}{T_e}\right\}\right] (\mathrm{cm^{-3}sec^{-1}}), \tag{3}$$

$$\xi = 2(2\ell+1) - (\mu+1) + 2\sum_{m=l+1}^{n-1}(2m+1), \tag{4}$$

where

Z_{ij}^{ff}: equivalent ion charge concerning bremsstrahlung,
$\overline{g_{ff}}$ and $\overline{g_{fb}}$: Gaunt factor[2],
χ_H: ionization potential of hydrogen (=13.6 eV),
χ_{ij}: ionization potential from the ground state[3),4)],
ξ: the number of unoccupied energy levels in $n\ell$-subshell,
n: principal quantum number in the ground state,

μ: the number of equivalent electrons in the $n\ell$-subshell after the recombination,

provided that after recombination radiation, ions (ion density n_{ij}) with ion charge Z_{ij} and configuration $n\ell^{\mu-1}$ change to those with ion charge $Z_{ij}-1$ and configuration $n\ell^{\mu}$. The energy spectrum of soft X-ray radiation from the plasma with impurity is as follows:

$$\left(\frac{\Delta I}{\Delta E}\right)_{\text{total}}=\left(\frac{\Delta I}{\Delta E}\right)_{\text{p}}^{\text{ff}}+\sum_{\text{i}}\sum_{\text{j}}\left\{\left(\frac{\Delta I}{\Delta E}\right)_{\text{ij}}^{\text{ff}}+\left(\frac{\Delta I}{\Delta E}\right)_{\text{ij}}^{\text{fb}}\right\}, \tag{5}$$

where i is the index of impurity ion (i=O, Fe, Mo, and so on) and j is the index of ion charge.

2.2. Principle of measurements

The energy dependence of soft X-ray photon number $n(E)$ can be obtained by PHA system with Multi-Channel Analyzer (MCA). The relation between $n(E)$ and $(\Delta I/\Delta E)_{\text{total}}$ is as follows:

$$\left(\frac{\Delta I}{\Delta E}\right)_{\text{total}}=\frac{1}{S(E)}\frac{En(E)}{L\Delta S\Delta\Omega}, \tag{6}$$

where

$S(E)$: effective detecting efficiency of soft X-ray detector,

ΔS: cross section of plasma viewed by detector,

L: sight-length of plasma,

$\Delta\Omega$: solid angle viewed by detector.

Abel inversion must be taken into account, since soft X-ray detector measures the integrated value along plasma cross section. But the contribution from low-electron-temperature region in the plasma periphery is negligible because of energy dependence of soft X-ray (exponential function of photon energy). Therefore the detector may detect only soft X-ray from the high-temperature core region. The propriety of this assumption is discussed in section 5.

The electron temperature can be estimated from the gradience of the continuous spectrum plotted on the semi-log graph because of the exponential dependence $\exp(-E/T_e)$ of both bremsstrahlung and recombination radiation. In this case we must adopt the gradience of the continuous spectrum in the energy region where the influence of line radiation is very small. And the contribution of high-energy tail due to the high energy electrons (runaway electrons) must be removed.

2.3. Calculation of ζ and Z_{eff}

The ratio ζ of the measured intensity to the calculated intensity of bremsstrahlung due to pure hydrogen (called "enhancement factor")[5] and the ratio $(\gamma$-1) of recombination radiation due to impurity to bremsstrahlung due to impurity are calculated. The value of Z_{eff} can be calculated from ζ and γ.

The ratio γ is a function of electron temperature and ionization state

of impurity,

$$\gamma(T_e, Z_{ij}) = \frac{(\Delta I/\Delta E)_{ij}^{ff} + (\Delta I/\Delta E)_{ij}^{fb}}{(\Delta I/\Delta E)_{ij}^{ff}} \equiv \gamma_{ij}. \tag{7}$$

The ratios γ_{ij} for the principal impurties oxygen (O) and iron (Fe) are shown in Figs. 1 (a) and (b), respectively. Equation (5) in the previous subsection 2.1 becomes

$$\left(\frac{\Delta I}{\Delta E}\right)_{total} = \left(\frac{\Delta I}{\Delta E}\right)_{p}^{ff} + \sum_i \sum_j \gamma_{ij} \left(\frac{\Delta I}{\Delta E}\right)_{ij}^{ff}. \tag{8}$$

And the enhacement factor ζ becomes,

$$\zeta = \frac{n_p}{n_e} Z_p^2 + \sum_i \sum_j \gamma_{ij} \frac{n_{ji}}{n_e} (Z_{ij}^{ff})^2. \tag{9}$$

By substituting the neutral condition

$$n_e = Z_p n_p + \sum_i \sum_j Z_{ij} n_{ij} \tag{10}$$

into eq. (9), we obtain

$$\zeta = \frac{n_e - \sum_i \sum_j Z_{ij} n_{ij}}{n_e Z_p} Z_p^2 + \sum_i \sum_j \gamma_{ij} \frac{n_{ij}}{n_e} (Z_{ij}^{ff})^2. \tag{11}$$

By assuming that the impurity is only one species and ionization state of impurity is only one state, eq. (11) is simplified as

$$\zeta = Z_p - \frac{Z_{ij} n_{ij}}{n_p} Z_p + \gamma_{ij} \frac{n_{ij}}{n_e} (Z_{ij}^{ff})^2. \tag{12}$$

Then the concentration of impurity is

$$\frac{n_{ij}}{n_e} = \frac{\zeta - Z_p}{\gamma_{ij}(Z_{ij}^{ff})^2 - Z_{ij} Z_p} \tag{13}$$

From the definition, the effective ion charge Z_{eff} is,

$$Z_{eff} \equiv \frac{n_p Z_p^2 + \sum_i \sum_j n_{ij} Z_{ij}^2}{n_e} \tag{14}$$

By assuming similarly as in eq. (12) and substituting eq. (13), we obtain

$$Z_{eff} = Z_p + \frac{(\zeta - Z_p) Z_{ij} (Z_{ij} - Z_p)}{\gamma_{ij}(Z_{ij}^{ff})^2 - Z_{ij} Z_p} \tag{15}$$

2.4. Line spectra in energy region of soft X-ray

In order to know the kind of impurities, we must identify line spectra which are radiated when electrons transit from levels to another lower levels. In energy range of soft X-ray (1 keV-30 keV), there are lines of iron (Fe) and molybdenum (Mo), and no lines of oxygen (O)[6),7)].

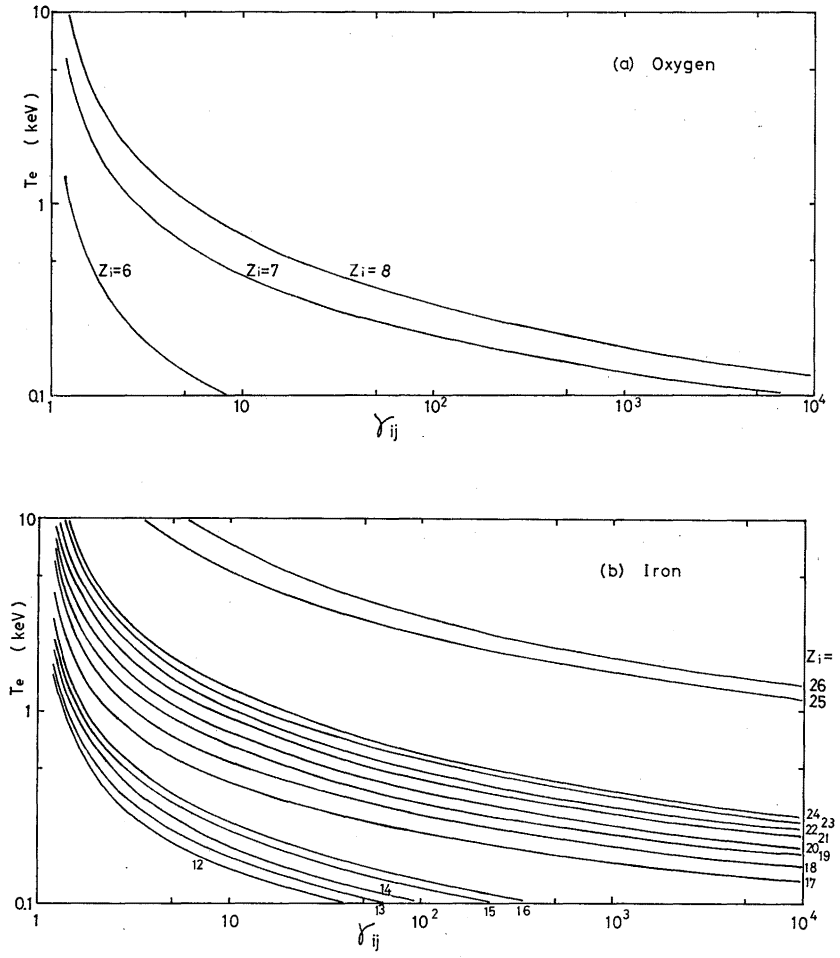

Fig. 1 The ratio γ_{ij} of the sum of bremsstrahlung recombination radiation to bremsstrahlung for oxygen (a) and iron (b).

3. Experimental equipment

The TRIAM-1 tokamak is a high-magnetic-field tokamak for experimental studies of confinement of high-density plasma and turbulent heating[8),9)]. The device parameters and plasma parameters of TRIAM-1 are summarized in Tables 1(a) and (b), respectively. Figure 2 shows the plan view of TRIAM-1 with diagnostic instruments and pumping system.

Soft X-ray falls off in the air. So the path of soft X-ray must be evacuated to less than 10^{-4} Torr. Figure 3 shows the vacum chamber,

Table 1(a) Device parameters of TRIAM-1.

Major radius	$R_0=25.4$	cm
Limiter radius	$a_L=4$	cm
Toroidal field	$B_T=40$	kG
Vertical field	$B_V=1000$	G
Horizontal field	$B_H=50$	G
Base pressure	$P_B=2\times10^{-10}$	Torr

Table 1(b) Typical plasma parameters of TRIAM-1 in case of only joule heating.

Plasma current	$I_P=21$	kA
Loop voltage	$V_{Loop}=4$	V
Electron density	$\overline{n_e}=2\times10^{13}$	cm^{-3}
Electron temperature	$T_{e0}=250$	eV
Ion temperature	$T_{i0}=140$	eV

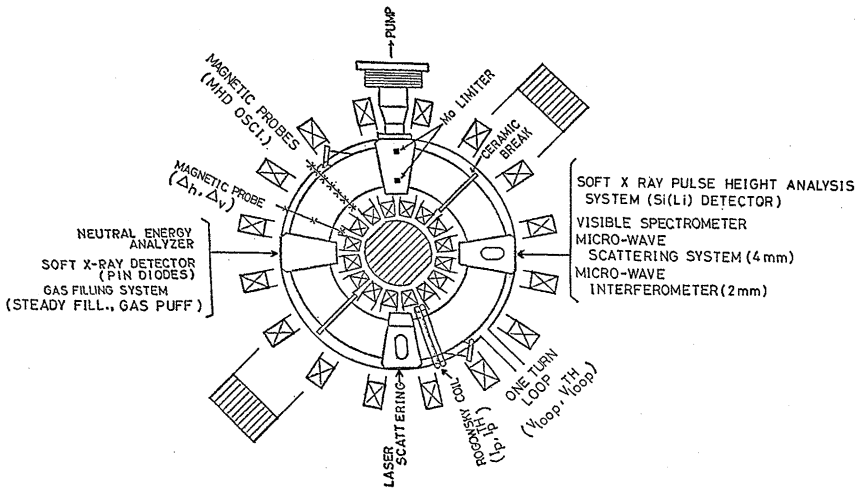

Fig. 2 Plan view of TRIAM-1 with diagnostic instruments and pumping system.

which plays a role of the attachment between TRIAM-1 and soft X-ray detector, and the pumping system of PHA system. This system has a movable base which can rotate around the turning point. So we can measure the radial profile of soft X-ray radiation.

3.1. Collimator and absorber

The collimator determines the plasma cross section and the solid angle viewed by the detector. This collimator consists of slit 1 on the plasma side and slit 2 on the detector side which are made of stainless steel (1 mm thick). Table 2 shows the plasma cross section, the solid angle, and the spatial resolution for various combinations of slit 1 and slit 2.

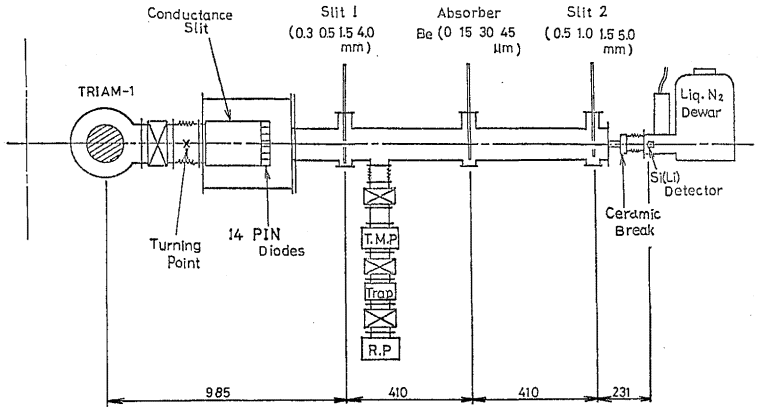

Fig. 3 Schematic diagram of TRIAM-1, vacuum chamber and pumping system of pulse height analysis system of soft X-ray.

Table 2 Geometrical constants for various combination of slit 1 and slit 2. D_1 and D_2 (mm): diameters of slit 1 and slit 2, respectively, ΔS (mm²): plasma cross section, $\Delta\Omega$ (ster): solid angle and Δr_m (cm): spatial resolution.

D_1	D_2	ΔS	$\Delta\Omega$	Δr_m
0.3	0.5	1.25	6.02×10^{-8}	±0.063
	1.0	2.72	2.41×10^{-7}	±0.093
	1.5	4.75	5.42	±0.123
	5.0	34.82	6.02×10^{-6}	±0.333
0.5	0.5	2.27	6.02×10^{-8}	±0.085
	1.0	4.15	2.41×10^{-7}	±0.115
	1.5	6.60	5.42	±0.145
	5.0	39.57	6.02×10^{-6}	±0.355
1.5	0.5	11.94	6.02×10^{-8}	±0.195
	1.0	15.90	2.41×10^{-7}	±0.225
	1.5	20.42	5.42	±0.255
	5.0	67.89	6.02×10^{-6}	±0.465
4.0	0.5	69.36	6.02×10^{-8}	±0.470
	1.0	78.50	2.41×10^{-7}	±0.500
	1.5	88.20	5.42	±0.530
	5.0	172.41	6.02×10^{-6}	±0.741

The absorber, which is made of beryllium (15, 30 and 45 μm thick), is used to remove the photons whose energy is less than 1 keV. The detector has an entrance window of beryllium in order to keep the detector in vacuum of 10^{-5} to 10^{-6} Torr and a dead layer of sillicon. These also play a role of an absorber.

3.2. Soft X-ray detector

Silicon lithium drifted detector (Si(Li) detector) delivered by ORTEC is used as soft X-ray detector. The specification of this detector is summarized in Table 3. This detector transforms the photon energy to the electric signal. Soft X-ray coming into the window enters into the

Si(Li) crystal through gold foil and silicon dead layer. Soft X-ray absorbed in sensitive area of the detector is transformed to electron-hole pair with rate of 3.6 eV per pair. So the transformation function is,

$$W(E)=1.6\times10^{-19}\frac{E}{3.6}\left\{1-\exp(-\mu_D\rho_D d_D)\right\} \quad \text{(coulomb)}, \tag{16}$$

where

μ_D: absorption coefficient of silicon (cm^2/g),
ρ_D: mass density of silicon (g/cm^3),
d_D: thickness of sensitive area of detector (cm).

And the intensity of soft X-ray falls off also by the effect of absorber and so on, and its characteristics is as follows,

$$F(E)=\exp(-\sum_{i=1}^{N}\mu_i\rho_i d_i), \tag{17}$$

where μ_i: absorption coefficient of material i (cm^2/g),
ρ_i: mass density of material i (g/cm^3),

Table 3 Specification of Si(Li) soft X-ray detector.

Type	ORTEC 7513 S-6300
Crystal	ϕ 6.0mm×t 5.32 mm
Entrance window	Beryllium: 0.0125 mm
	Gold: ~200 Å
Silicon dead layer	~0.1 μm
Bias voltage	−1000 V
Energy resolution	200 eV FWHM at 5.9 keV
Connection flange	IFC 070

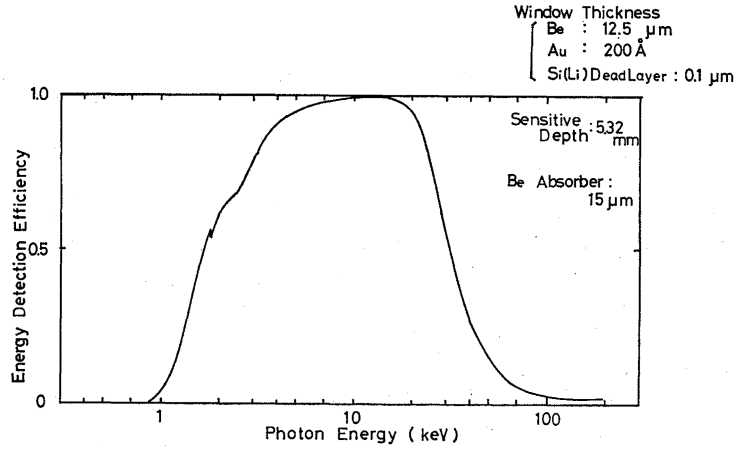

Fig. 4 Effective detecting efficiency of Si(Li) soft X-ray detecting system using 15 μm beryllium.

d_i: thickness of material i (cm).

Therefore the effective detecting effieciency using 15 μm beryllium versus the photon energy is as follows (Fig. 4),

$$S(E)=\{1-\exp(-\mu_D\rho_D d_D)\}\exp\{-\sum_{i=1}^{N}\mu_i\rho_i d_i\}. \quad (18)$$

3.3. Electric circuit system

Figure 5 shows the block diagram of electric circuit system. Negative pulse (rising time is 10–650 ns and falling time is about 40 μs) which is proportional to soft X-ray energy comes out of the preamplifier. This pulse enters into the spectroscopy amplifier and shaped into the gaussian pulse (the pulse height of which is proportional to soft X-ray energy) and the square pulse (the pulse width of which is 0.5 μs), and go out of "slow out" and "fast out" of the spectroscopy amplifier, respectively.

The duration time of TRIAM-1 tokamak plasma is about 10 msec. So in order to know temporal evolution of electron temperature and so on, the experimental data are collected during times set by micro-computer, Δt_1, Δt_2. Δt_3 and Δt_4.

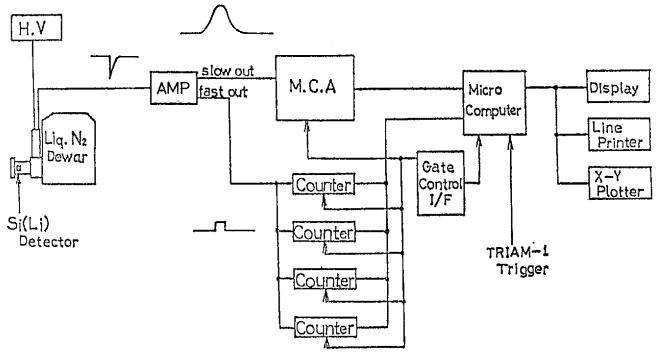

Fig. 5 Block diagram of electric circuit system of pulse height analysis system of soft X-ray.

3.4. Calibration of PHA system

The calibration of PHA system, i.e. the relation of soft X-ray energy and the channel number of MCA, was made using radio isotope ^{55}Fe.

Soft X-ray of 5.898 keV and 6.489 keV from ^{55}Fe is detected by Si (Li) detector and analyzed by MCA. As a result a spectrum with two peaks is obtained. We obtain the energy per channel from the positions of these peaks. Figure 6 shows the energy spectrum of soft X-ray from the radio isotope ^{55}Fe.

The energy resolution of this system is about 250 eV FWHM at 5.898

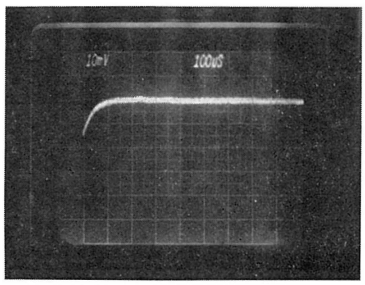

(a) output of the preamp.
10 mV/div.
100 μs/div

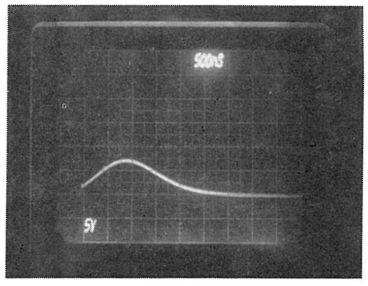

(b) output of the amp.
5 V/div.
500 ns/div.

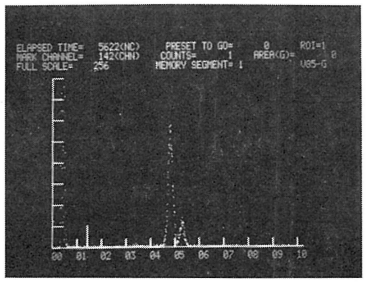

(c) M.C.A. display
$Mn\ K\alpha$ 5.898 KeV
$Mn\ K\beta$ 6.489 KeV

Fig. 6 Output of preamplifier and spectroscopy amplifier and Mn K-line spectrum of ^{55}Fe on display of MCA in energy calibration.

keV. On the other hand, the energy resolution of only detector has the energy dependence,

$$\Gamma_{\mathrm{FWHM}} = \{(\Gamma_{\mathrm{noise}})^2 + (2.35\sqrt{\varepsilon FE})^2\}^{1/2}, \tag{19}$$

where $\varepsilon = 3.6$ eV,

$F = 0.125$,

$\Gamma_{\mathrm{noise}}(\tau)$: function of shaping time constant τ.

From this formula, Γ_{FWHM} at 10, 20 and 30 keV of soft X-ray are 224, 274 and 316, respectively. However, the energy region measured is about 1 keV-5 keV, so the energy resolution of this detector is about 200 eV.

4. Experimental results

4.1. Experimental condition

The discharge condition of TRIAM-1 tokamak is selected for measurements of energy spectrum of soft X-ray radiation as follows:

i) Toroidal field $B_T = 23-28$ kG,

ii) Filling pressure $P_f = 1.12-1.16\times10^{-3}$ Torr (H_2),

and the principal plasma parameters are as follows,

i) Plasma current $I_p = 10-35$ kA,

ii) Loop voltage $V_{Loop} = 2-6$ V,

iii) Electron density $\overline{n_e} = 2-3\times10^{13}$ cm^{-3}.

Figure 7 shows the waveforms of plasma current, loop voltage and electron density. The temporal evolution, the radial profile, and the plasma current dependence were measured in case of only joule heating.

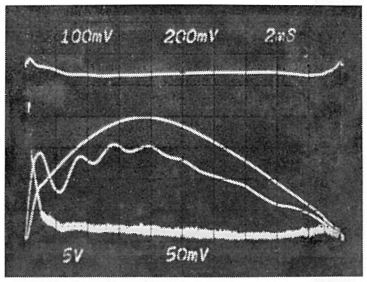

Ip (5.84 kA/div.)

Vloop (10 V/div.)

(2 ms/div.)

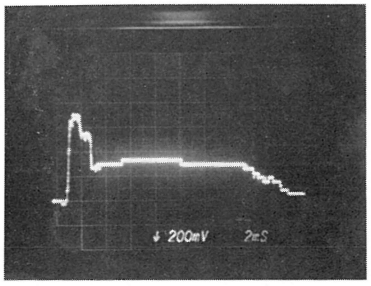

$\overline{n}_e$(1.6x10^{13}cm^{-3}/div.)

(2 ms/div.)

Fig. 7 Temporal evolution of plasma parameters.
I_p: plasma current, V_{Loop}: loop voltage, and $\overline{n_e}$: average electron density.

4.2. Energy spectrum of soft X-ray

Figure 8 shows the energy spectrum of the photon number (lowest

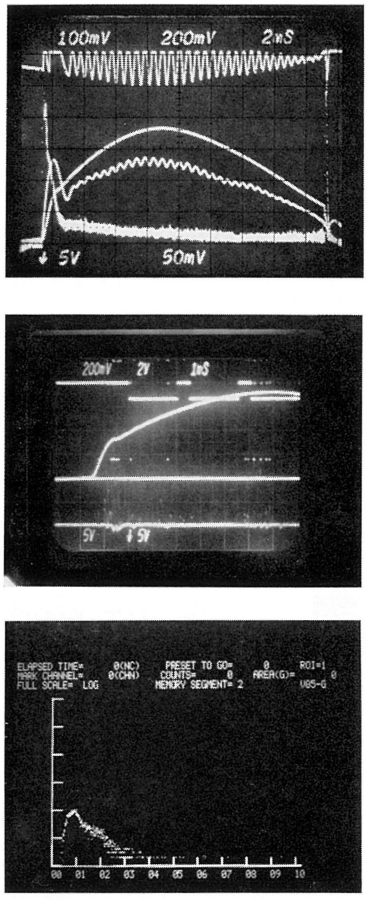

I_p (5.84kA/div.)

V_{loop} (10 V/div.)

Gate signal (5V/div.)

Inhibit signal (5V/div.)

Amp output (0.5V/div.)

M.C.A. display
Time : 8 – 10 msec
100 channel/div.

Fig. 8 Typical waveforms of signals.
(a) waveforms of plasma current and loop voltage,
(b) gate signal, inhibit signal and output of spectroscopy amplifier, and (c) the energy dependence of photon number $n(E)$ on the display of MCA.

figure) and Fig. 9 shows the typical energy spectrum of soft X-ray radiation. From this spectrum:

i) There are peaks of line radiation due to impurity at about 2.2 and about 2.8 keV. It seems that the peak at about 2.8 keV is the L-line of molybdenum.

ii) The energy spectrum of soft X-ray radiation consists of the bulk part and the high-energy-tail part. So as we obtain electron temperature, the high-energy tail must be subtracted from the bulk. And the contribution of line radiation must be removed. Therefore the energy region of 1.3 keV $< E <$ 1.9 keV is taken into account.

iii) The ratio n_e(tail)/n_e(bulk) of high-energy electron density to

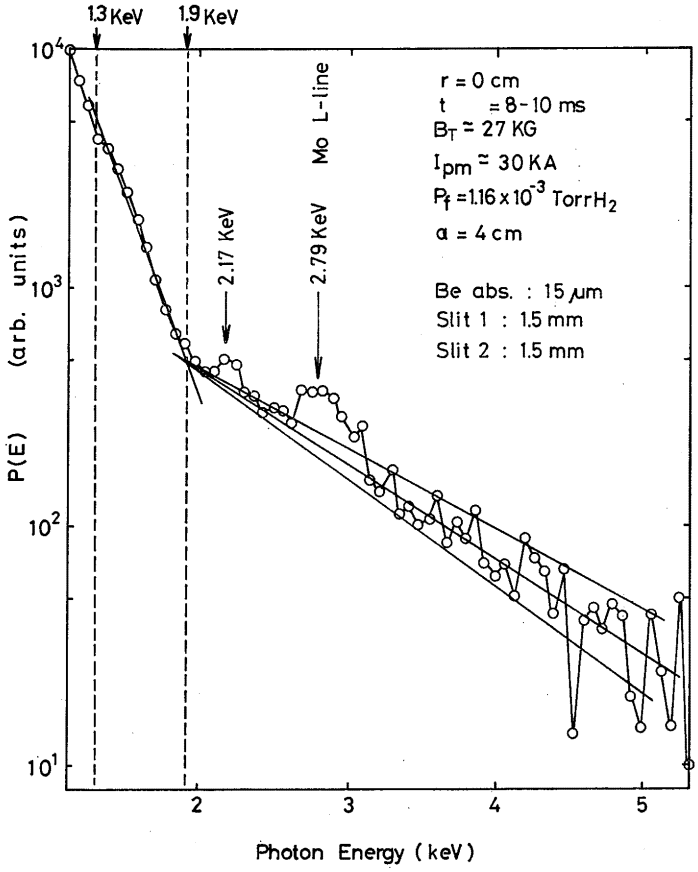

Fig. 9 Energy spectrum $P(E)$ of soft X-ray radiation.

bulk electron density and the effective temperature T_e(tail) can be obtained. In case of Fig. 9 the former is about 0.3% and the latter is 1.1 ± 0.2 keV.

4.3. Electron temperature measurements of bulk electrons

Figure 10 shows temporal evolution of bulk electron temperature and that measured by Thomson scattering method at plasma center. Both show the good agreement.

Figures 11 (a) and (b) show radial profile of the bulk electron temperature during Δt_2 and Δt_3, respectively. Figure 11 (b) shows the good agreement of this method and Thomson scattering, but there is a bit of difference, due to the difference of vertical profile and horizontal profile.

Figure 12 shows the dependence of electron temperature at plasma center on the plasma current. From this figure electron temperature

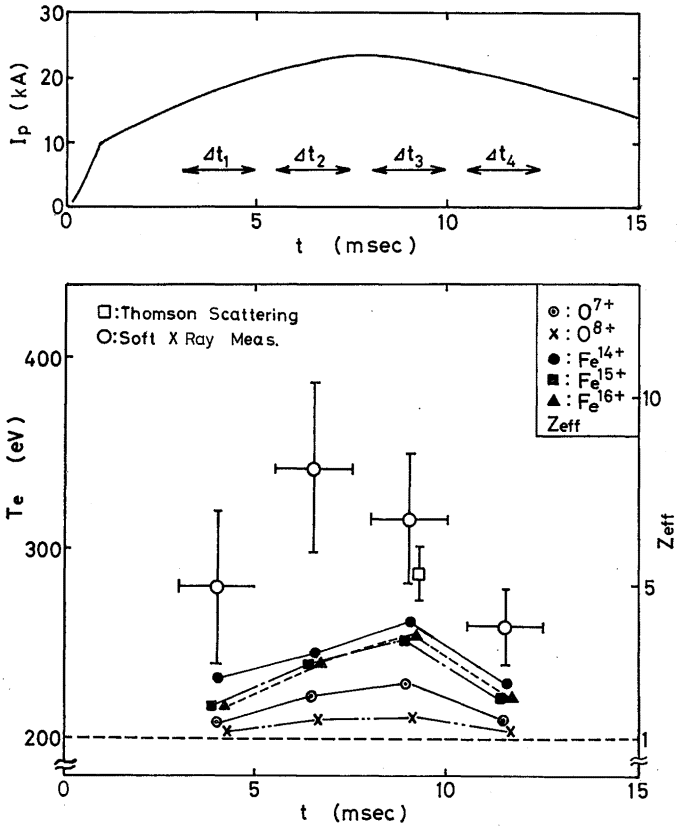

Fig. 10 Temporal evolution of electron temperature $T_{e0}(t)$ and $Z_{eff}(t)$ at plasma center.

increases in proportion to the plasma current I_p as in usual tokamak plasma.

4.4. Enhancement factor

Figure 13, 14 and 15 show temporal evolution, radial profile and plasma current dependence of enhacement factor ζ, respectively. In these figures the value of ζ is 10 to 160 and this value is the same as other tokamaks[1),10),11)]. The value $\zeta(r)$ near center of plasma is about constant and is large in the plasma periphery. This means the quantity of soft X-ray radiation from the impurity is large in the plasma periphery.

4.5. Effective ion charge Z_{eff}

The followings are assumed concerning impurity in order to calculate Z_{eff} from ζ by using eq. (15):

1) only one species of impurity exists,
2) only one ionization state of impurity exists.

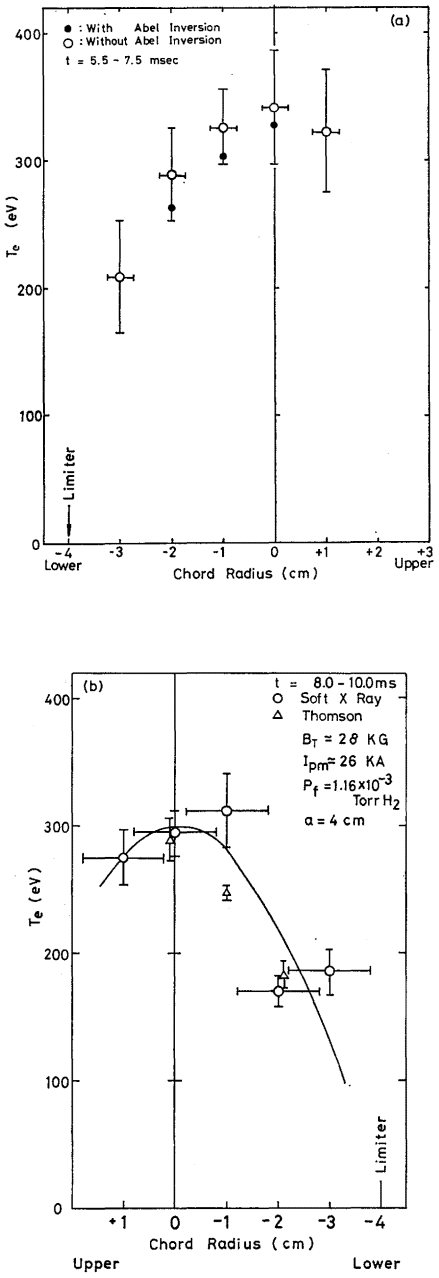

Fig. 11 Radial profile $T_e(r)$ of electron temperature (a) during Δt_2 and (b) during Δt_3.

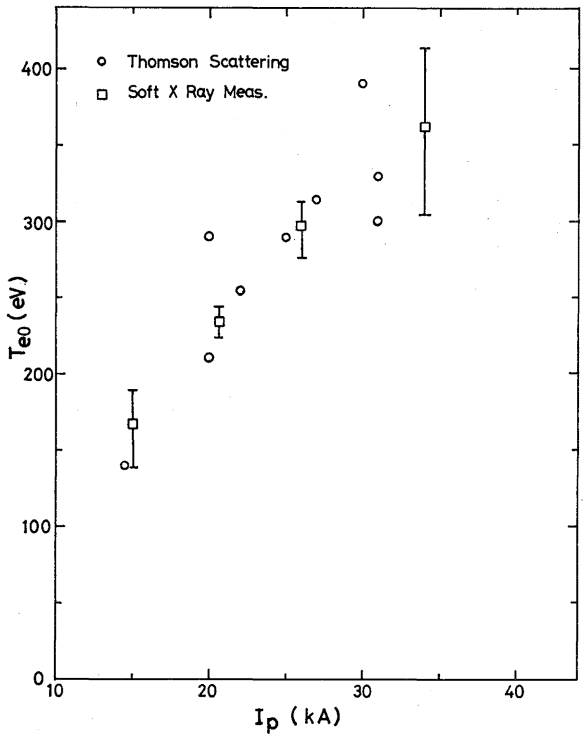

Fig. 12 Plasma current dependence of electron temperature T_{e0}.

The ionization state of impurity is detemined by corona equilibrium model. In the TRIAM-1 tokamak plasma, the pcincipal impurities are surmised oxygen (O) and iron (Fe), and these ionization state are O^{7+}, O^{8+}, Fe^{14+}, Fe^{15+} and Fe^{16+}.

Temporal evolution of Z_{eff} (0) is shown in Fig. 10. Figure 16 shows radial profile $Z_{eff}(r)$. Figure 17 shows the plasma current dependence of Z_{eff} and $Z_{eff}^{cond.}$ calculated from the conductivity of plasma. From these figures the value of Z_{eff} is 1 to 4 and agrees with $Z_{eff}^{cond.}$. By using eq. (13) the ratio of impurity ion and electron density is calculated to be several % for oxygen (O) and less than 1% for iron (Fe).

5. Discussions

5.1. Spatial profile

Abel inversion was not considered in the calculation of the energy spectrum of soft X-ray radiation $(\Delta I/\Delta E)_{total}$ from the energy spectrum of the photon number $n(E)$. Here we perform Abel inversion. In this

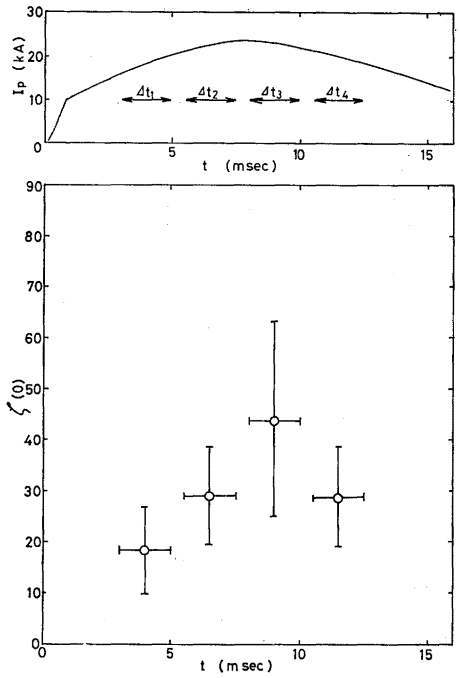

Fig. 13 Temporal evolution of enhancement factor $\zeta(0)$.

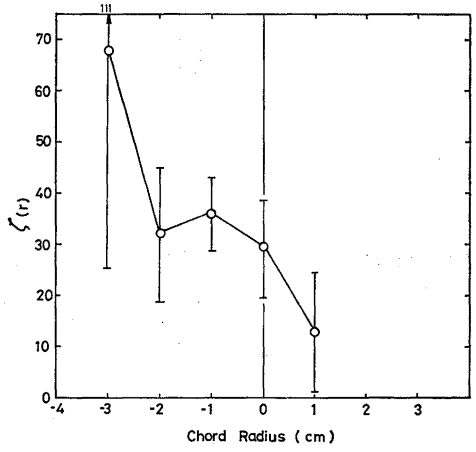

Fig. 14 Radial profile of enhancement factor ζ.

Abel inversion plasma is divided into 5 layers. The result is plotted in Fig. 11 (a). There is no difference between the result with and without Abel inversion.

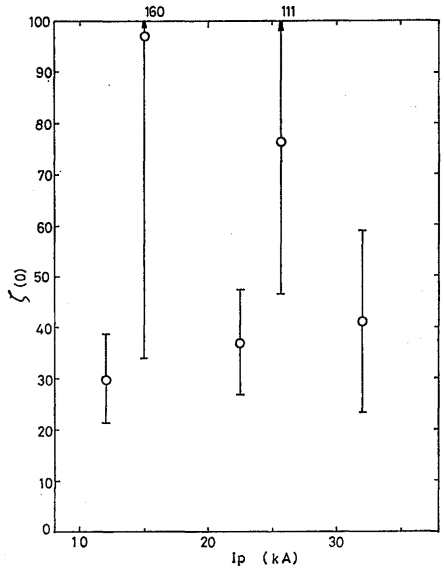

Fig. 15 Plasma current dependence of enhancement factor $\zeta(0)$.

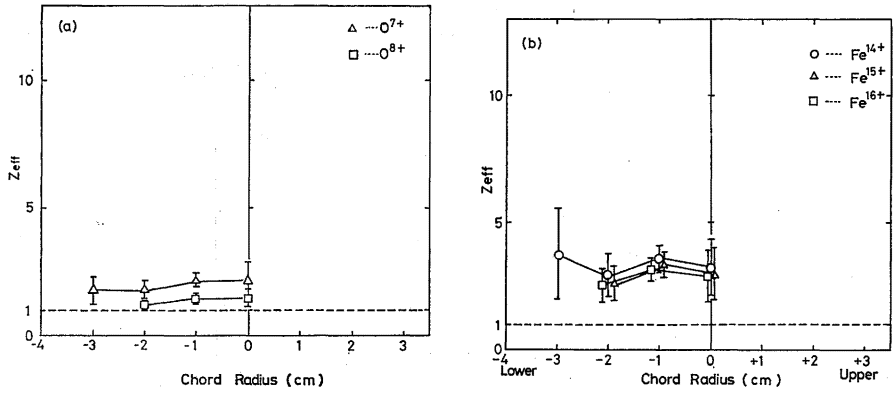

Fig. 16 Radial profile of $Z_{eff}(r)$ for oxygen (a) and iron (b).

5.2. High-energy tail and runaway electrons

The electron temperature was determined assuming Maxwellian plasma. In practice, however, electrons are not Maxwellian, i.e. the energy spectrum is predicted to be distorted from Maxwellian distribution.

In case of energy spectrum in Fig. 9, the discharge condition is plotted in $\overline{n}_e - \langle j \rangle$ diagram[12] together with the values of other tokamaks in Fig. 18. A solid line shows the threshold of runaway discharges,

$$\langle j \rangle / \overline{n}_e \sim 1.5 \times 10^{-11} \quad \text{(Acm)}. \tag{20}$$

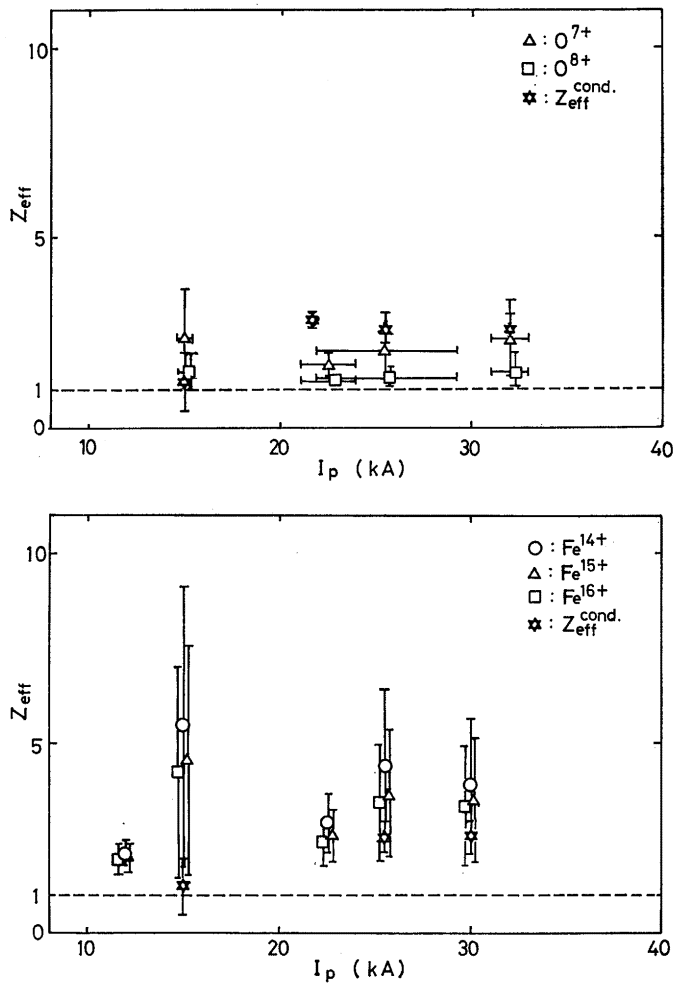

Fig. 17 Plasma current dependence of Z_{eff} (0) and $Z_{\text{eff}}^{\text{cond.}}$ derived from conductivity for oxygen and iron.

In this way runaway electrons characterizes the non-Maxwellian distribution in soft X-ray measurements. In Fig. 9 high-energy tail due to runaway electrons is identified clearly.

5.3. Design of measuring apparatus

The performance, the measuring limitation and the reliance are determined by

i) spatial resolution,
ii) responce time,
iii) energy resolution,

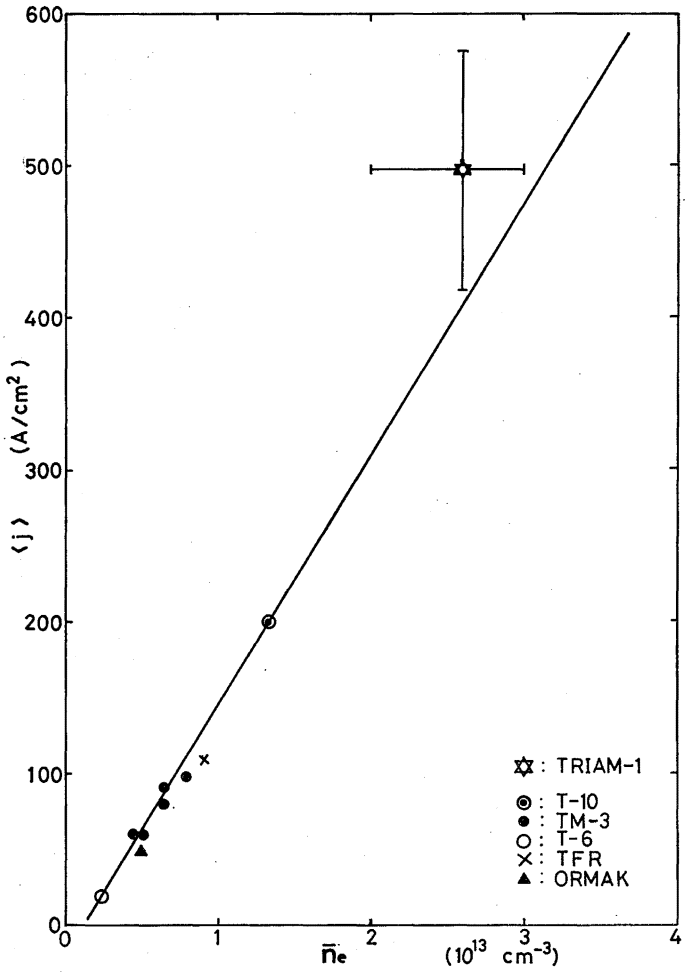

Fig. 18 Plasma current density $\langle j \rangle$ versus electron density $\overline{n_e}$. Runaway discharges occur often above the solid line.

iv) capability of temporal evolution measurement,
v) capablilty of spatial profile measurement.

Here we discuss about i) and ii).

There are two kinds of spatial resolution; the one is Δr_m determined by the mechanical structure and the another is Δr_p determined by the profiles of electron temperature and electron density. The value Δr_m was described in subsection 3.1. The value Δr_p is defined as the distance to the place where the intensity decreases to 1% of the peak. Table 4 shows the spatial resolution Δr_m and Δr_p at chord radii of 1, 2 and 3 cm, where $T_e = T_{e0} \times (1-(r/a_L)^2)^2$ and $n_e = n_{e0}(1-(r/a_L)^2)^{1/2}$. Since $\Delta r_m < \Delta r_p$

Table 4 Spatial resolution.

Chord radius	Δr_m	Δr_P
0 cm	±0.25 cm	±1.80 cm
1	〃	±1.67
2		±1.50
3	±0.74	±0.60

$< a_L$ (a_L is limiter radius), the spatial resolution in the viewing direction of the detector is bad and Abel inversion is in need. But as mentioned in the previous subsection 5.1., since the difference between the result with Abel inversion and that without it is negligible, Δr_m is considered to be the spatial resolution.

The plasma duration time of TRIAM-1 is about 10 msec. This time is divided into 4 blocks, so the measuring time is about 1–2 msec. In addition it is desirable to collect the data with the number of shots as small as possible from a point of reproducibility of plasma. Accordingly the response of the total system must be very fast. Here the preamplifier and MCA are in problem. In the preamplifier energy resolution is contrary to response time. The faster the response is, the broader the energy resolution is. However, the preamplifier used in this system has the finest energy resolution of 200 eV of all solid state detectors and the fastest response of about 10^5 pulse/sec. And MCA has a high frequency clock of 100 MHz in ADC. So this system is considered to have the fastest response.

6. Conclusions

Soft X-ray pulse height analysis system has been designed and constructed, and measurements of spatial profile and temporal evolution for electron temperature and effective ion charge Z_{eff} are possible.

The following results have been obtained:

i) Electron temperature by soft X-ray pulse height analysis agrees well with that by Thomson scattering method.

ii) Electron temperature increases in proportion to plasma current as in usual tokamak plasma.

iii) The value of enhancement factor ζ is 10–160 which is the same value as other tokamaks.

iv) The value of Z_{eff} is 1–4 and higher than $Z_{eff}^{cond.}$ derived from conductivity. This is because $Z_{eff}^{cond.}$ is estimated lower due to the existence of high-energy electrons (runaway electrons).

v) We obtained not only the information concerning bulk electrons but also that of high-energy electrons (runaway electrons).

vi) Spatial profile of Z_{eff} is flat except plasma periphery.

Acknowledgements

The authors would like to express their gratitude to Professor N. Yajima for his continuous encouragements, to Dr. K. Matsuoka and Dr. M. Sato for their technical advice, and to Mr. S. Kawasaki and Mr. H. Nakashima for their technical assistance in the experiments.

References

1) Von Goeler, S., Stodiek, W., Eubank, H., Fishman, H., Grebenshchikov, S. and Hinnov, E.: *Thermal X-Ray Spectra and Impurities in the ST Tokamak*, Nucl. Fusion **15** (1975) 301.
2) Karzas, W. J. and Latter, R.: Astrophys. J. Suppl. **55** (1961) 167.
3) Carison, D. A., et al.: Atomic Data **2** (1970) 63.
4) Allen, C. W.: *Astrophysical Quantities* (William Clowes and Sons, London, 1973).
5) Sesnic, S.: IPP III/22 (1976).
6) Breton, C., De Michelis, C. and Mattioli, M.: EUR-CEA-FC-853 (1976).
7) Schwob, J. L., Klapisch, M., Finkenthal, M., Schweitzer, N. and TFR Group: *Identification of MoXV to MoXXXIII in the Soft X-Ray Spectrum of the TFR Tokamak*, EUR-CER-FC-887 (1977).
8) Hiraki, N., Itoh, S., Kawai, Y., Toi, K., Nakamura, K. and Mitarai, O.: *Confinement of Ohmically Heated Plasmas and Turbulent Heating in High-Magnetic-Field Tokamak TRIAM*-1, Reports of Research Institute for Applied Mechanics **27** No. 85 (1979) 85.
9) Toi, K., Hiraki, N., Nakamura, K., Mitarai, O., Kawai, Y. and Itoh, S.: *Observation of Bulk-Ion Heating in a Tokamak Plasma by Application of Positive and Negative Current Pulses in TRIAM*-1, Nucl. Fusion **20** No. 9 (1980) 1169.
10) Equipe TER: *Electron Temperature and Z_{eff} Measurements in the Hot Plasma of TFR by Soft-X-Ray Analysis*, Nucl. Fusion **17** No. 2 (1977) 213.
11) Axon, K. B., Paul, J. W. M. and Prentice, R.: *Soft X-Ray Measurements of the Impurity Density in DITE*, Nucl. Fusion **19** No. 8 (1979) 1003.
12) Knoepfel, H.: *Runaway Electrons in Toroidal Discharges*, Nucl. Fusion **19** No. 6 (1979) 785.

(Received April 27, 1981)